PCCP

Accepted Manuscript

ROYAL SOCIETY OF CHEMISTRY

www.rsc.org/pccp

Isotope-edited FTIR reveals distinct aggregation and structural behaviors of unmodified and pyroglutamylated amyloid β peptides

Greg Goldblatt[a], Jason O. Matos[b], Jeremy Gornto[c] and Suren A. Tatulian*[d]

[a]*Biomedical Sciences Graduate Program, University of Central Florida, Orlando, FL, USA,* [b]*Biotechnology Graduate Program, University of Central Florida, Orlando, FL, USA (currently at Graduate Program in Biochemistry and Biophysics, Brandeis University, Waltham, MA, USA),* [c]*Undergraduate student, University of Central Florida, Orlando, FL, USA (currently at Pharmacy PhD Program, Ohio State University, Columbus, OH, USA),* [d]*Department of Physics, University of Central Florida, Orlando, FL, USA.*

*Corresponding author: Department of Physics, Physical Sciences Room 456, University of Central Florida, 4111 Libra Drive, Orlando, Florida 32816-2385, USA. Tel.: 407-823-6941; Fax: 407-823-5112; E-mail: statulia@ucf.edu

Table of contents entry

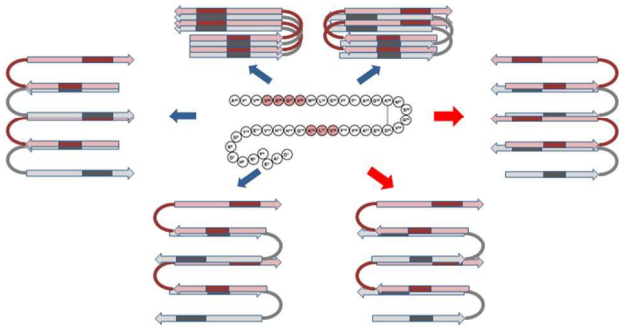

Isotope-edited FTIR has been used to structurally characterize the early oligomers of amyloid β peptide $A\beta_{1\text{-}42}$ and the pyroglutamylated peptide $A\beta pE_{3\text{-}42}$.

Amyloid β peptide (Aβ) is causatively associated with Alzheimer's disease (AD), and N-terminally truncated and pyroglutamylated Aβ peptides (AβpE) exert hypertoxic effect by an unknown mechanism. Recent evidence has identified the prefibrillar oligomers of Aβ, not the fibrils, as the prevalent cytotoxic species. Structural characterization of Aβ and AβpE oligomers is therefore important for better understanding of their toxic effect. Here we have used isotope-edited Fourier transform infrared (FTIR) spectroscopy to identify the conformational changes in $A\beta_{1\text{-}42}$ and $A\beta pE_{3\text{-}42}$ upon aggregation, individually and in 1:1 molar combination. During the first two hours of exposure to aqueous buffer, the peptides undergo transition from mostly α-helical to mostly β-sheet structure. Data on peptides ^{13}C,^{15}N-labeled at $K^{16}L^{17}V^{18}$ or $V^{36}G^{37}G^{38}V^{39}$ allowed construction of structural models for the monomer and early oligomers. The peptide monomer comprises a β-hairpin that involves residues upstream of the $K^{16}L^{17}V^{18}$ sequence and an N-terminal α-helix. The oligomers form by non-H-bonding interactions between the β-strands of neighboring β-hairpins, in lateral or staggered manner, with the strands running parallel or antiparallel. Relative α-helical and β-sheet propensities of $A\beta_{1\text{-}42}$ and $A\beta pE_{3\text{-}42}$ depend on the ionic strength of the buffer, emphasizing the importance of ionic interactions in Aβ peptide structure and aggregation. It is inferred that N-terminal modification of $A\beta pE_{3\text{-}42}$ affects the helix stability and thereby modulates β-sheet oligomer formation. The data thus provide new insight into the molecular mechanism of Aβ oligomerization by emphasizing the role of the N-terminal transient α-helical structure and by identifying structural constraints for molecular organization of the oligomers.

List of abbreviations: Aβ, amyloid β peptide; AβpE, pyroglutamylated Aβ peptide; AD, Alzheimer's disease; APP, amyloid precursor protein, CD, circular dichroism; ER, endoplasmic reticulum; FTIR, Fourier transform infrared; HFIP, hexafluoroisopropanol; MD, molecular dynamics.

1. Introduction

Extracellular fibrillar deposits of Aβ peptide constitute a typical histopathological feature of AD.[1] Earlier studies suggested a causative role of the Aβ plaques in the disease.[2-4] However, recent evidence has identified the prefibrillar soluble oligomers of Aβ as the main neurotoxic entities.[5-13]

Although the mechanism underlying Aβ toxicity has not been determined, studies have led to various plausible pathways. The channel hypothesis suggests that Aβ forms pores and/or ion channels in the neuronal plasma membrane resulting in dysregulation of cellular homeostasis and cell death.[14-16] The endoplasmic reticulum (ER) pathway suggests that binding of Aβ to ER causes Ca^{2+} release ensued by abnormal activation of certain cytosolic enzymes and apoptotic cell death.[7,17-19] Altered mitochondrial dynamics is an early event in AD,[20] and is paralleled with recruitment of Aβ to mitochondria and subsequent apoptosis.[18,21-24] Finally, Aβ is known to bind to a range of receptors, entailing aberrant cell signaling events and leading to either necrosis or apoptosis.[10,25,26]

Aβ is derived from the amyloid precursor protein (APP), a bitopic protein in neuronal membranes, by proteolytic cleavage at the transmembrane region and the juxtamembrane extracellular region. The most prevalent forms are the 40- and 42-residue peptides. The fraction of $Aβ_{1-42}$ ($DAEFRHDSGY^{10}EVHHQKLVFF^{20}AEDVGSNKGA^{30}IIGLMVGGVV^{40}IA$) increases during AD,[27] suggesting its involvement in AD pathogenesis. Further processing of the peptide by amino- or carboxy-peptidases and enzymatic modifications result in an array of shorter peptides.[1,27,28] Among them, N-terminally truncated and pyroglutamylated (at Glu^3 or Glu^{11}) Aβ peptides (AβpE) have attracted much attention as they have been found in AD brains at significant quantities, reaching 50% of total Aβ peptide.[29-33] AβpE peptides have been shown to aggregate at increased rates[34-38] and to be hypertoxic as compared to the unmodified peptide.[29,34,39,40] Moreover, the presence of AβpE at low molar fractions (5% and below) substantially augmented the neurotoxicity of Aβ peptide.[29]

Solution NMR studies on peptides corresponding to the APP region that comprised the whole or part of $Aβ_{1-42}$ sequence, reconstituted in detergent micelles, revealed a disordered N-terminus and a flexible α-helix starting at $K^{16}L^{17}V^{18}$, with a bend involving the $V^{36}G^{37}G^{38}V^{39}$ segment.[41,42] These data implied that the Aβ sequence was mostly α-helical within the context of APP, before cleavage and release into the aqueous medium. On the other hand, the extracellular amyloid plaques are composed of fibrils of parallel, in-register cross β-sheet structure, where the β-strands are perpendicular and the intermolecular H-bonding is parallel to the fibrillar axis.[43-49] Obviously, the fibrillogenesis process involves a dramatic α-helix to β-sheet structural transition. Given that the prefibrillar oligomers exert the main cytotoxic effect,[5-13] analysis of the structural transitions during fibrillogenesis and characterization of the intermediate Aβ species are of paramount importance in understanding the structural basis of Aβ toxicity.

Solution and solid-state NMR studies have been conducted to determine the structure of $Aβ_{1-40}$ and $Aβ_{1-42}$ oligomers, where the oligomeric state has been stabilized by lyophilization,[11,49,50] sodium dodecyl sulfate,[11,51] co-solvents such as 10% hexafluoroisopropanol (HFIP),[52] or antibodies.[53] Despite the considerable differences in the structural details, the prefibrillar oligomers of $Aβ_{1-42}$ were found to form loosely packed antiparallel β-structures or mixed parallel/antiparallel β-sheets, as opposed to tightly packed parallel in-register β-sheets of the fibrils. Secondary structural differences between $Aβ_{1-42}$ fibrils and oligomers have also been

detected by other spectroscopic methods. Teplow and co-workers prepared low molecular weight $A\beta_{1-40}$ samples and used circular dichroism (CD) to monitor structural transitions upon aggregation.[54,55] The sum of α-helix + β-sheet fractions increased from monomers to tetramers and correlated with cytotoxicity, while the fibrils had zero α-helical content and showed low cytotoxicity.[55] Molecular dynamics (MD) studies on α-helix to β-sheet transition upon exposure of $A\beta_{1-42}$ or $A\beta_{1-40}$ to aqueous media predicted mixed α-helix/β-sheet intermediates as well.[56-58] Consistent with this, combined CD, solution NMR, and MD studies unveiled α-helix to β-sheet transition of $A\beta_{1-42}$ with increasing fraction of water in HFIP/H_2O.[59] Ono et al.[55] and Abedini and Raleigh[60] considered a mechanism where the initial aggregation occurs between the transient α-helical structures, which then convert to β-sheets. FTIR amide I bands of $A\beta_{1-42}$ oligomers showed a peak around 1645 cm^{-1}, suggesting irregular structure, which shifted to the β-sheet region of 1630 cm^{-1} upon induction of fibrillogenesis by heating.[49] Another FTIR analysis of $A\beta_{1-42}$ indicated formation of antiparallel β-sheets by the oligomers and parallel β-sheets by the fibrils.[61] Thus, the intermediate, prefibrillar Aβ species assume complex structures, involving α-helix, β-sheet, and irregular structures, which evidently contribute to Aβ toxicity.

Structural data on AβpE are scarce. Studies using CD, electron microscopy, and proteolysis-resistance showed that AβpE formed intermolecular β-sheets and fibrils that were shorter and thicker compared to fibrils of unmodified Aβ.[34-37] Solution NMR showed that $A\beta pE_{3-40}$ in trifluoroethanol/water (2:3) had a reduced α-helical propensity compared to $A\beta_{1-40}$.[62] This echoes with the findings of higher β-sheet propensity and faster aggregation of AβpE.[35,36] However, other studies opposed this notion by reporting that AβpE had similar content of β-sheet structure and aggregated slower than unmodified Aβ.[63,64] The structural distinctions between Aβ and AβpE, as well as the structural basis for hypertoxicity of AβpE remain poorly characterized.

Structural analysis of the prefibrillar oligomers of Aβ involved lyophilization, detergents or organic solvents (see above), all of which likely affect the peptide's structure. On the other hand, few studies have been conducted on AβpE, alone or in combination with the unmodified peptide. Our objective is to analyze the conformational transitions in Aβ and AβpE individually and in combination during aggregation in the absence of biologically impertinent components, and to help structurally characterize the toxic intermediates. Our earlier work indicated that, contrary to the doctrine that AβpE undergoes faster fibrillogenesis and β-sheet formation and thereby elicits a hypertoxic effect, AβpE is actually able to not only delay the aggregation of Aβ but also reverse the cross β-sheet structure of Aβ to α-helix.[65] Here we present a biophysical analysis of the structural transitions in $A\beta_{1-42}$ and $A\beta pE_{3-42}$ upon aggregation, individually and in 1:1 molar combination. We have studied unlabeled peptides, as well as peptides ^{13}C,^{15}N-labeled at regions $K^{16}L^{17}V^{18}$ or $V^{36}G^{37}G^{38}V^{39}$. The peptides dried from HFIP assume α-helical structure, and transfer to aqueous buffers initiates transition to more complex conformations, including β-sheet, β-turn, α-helix, and irregular structures. Analysis of $^{12}C{=}O$-$^{13}C{=}O$ and $^{13}C{=}O$-$^{13}C{=}O$ vibrational couplings provides structural constraints that lead to molecular models of peptide monomers and oligomers.

2. Experimental

2.1. Materials

Unlabeled $A\beta_{1\text{-}42}$ and $A\beta pE_{3\text{-}42}$ peptides were purchased from rPeptide (Bogart, GA, USA) and Innovagen (Lund, Sweden), respectively, and were > 97% pure. Uniformly ^{13}C,^{15}N-labeled amino acids were purchased from Cambridge Isotope Laboratories (Tewksbury, MA, USA) and sent to EZBiolab (Carmel, IN, USA), where the segmentally labeled peptides were synthesized. The final purity of these peptides was > 95%. Most chemicals including HFIP, salts, buffers were purchased from Fisher Scientific (Hanover Park, IL, USA) and Sigma-Aldrich (St. Louis, MO, USA).

2.2. Experimental procedures

The peptides were obtained from the vendors as lyophilized powder and stored at -20°C in tightly sealed vials. Samples for CD or FTIR experiments were prepared by first dissolving the peptides in HFIP at 50 μM concentration to disperse pre-existing aggregates, as described earlier.[66] In CD experiments, the peptide solution was contained in a 4 mm × 4 mm rectangular quartz cuvette and spectra were recorded on a J-810 spectropolarimeter (Jasco, Tokyo, Japan) at 25 °C. Then the solvent was removed under a gentle stream of nitrogen gas followed by desiccation for 30 min, and spectra of dry peptide were measured. Aqueous buffer was then added, accompanied with stirring with a magnetic stir bar, and CD spectra were measured consecutively for two hours to detect structural changes during aggregation. Samples of equimolar combination of $A\beta_{1\text{-}42}$ and $A\beta pE_{3\text{-}42}$ contained 25 μM of each peptide. Spectra were measured for blank buffers and subtracted from the sample spectra.

In FTIR experiments, 120 μL of 50 μM peptide solution in HFIP were placed on a circular CaF_2 FTIR window (32 mm in diameter, 3 mm thick) and dried as described above. The window was mounted on a sample holder and spectra were measured on a Vector-22 FTIR spectrometer (Bruker Optics, Billerica, MA, USA) equipped with a liquid nitrogen-cooled Hg-Cd-Te detector at 2 cm^{-1} nominal resolution at 25 °C, as described.[65] Following measurements of the spectra of dry peptides, the CaF_2 window was dismounted, placed horizontally, and 120 μL of D_2O-based buffer were added to the dry peptide. A 50 μm Teflon spacer and a second CaF_2 window were placed on top of the sample and tightly sealed. Consecutive FTIR spectra in the 4000 cm^{-1}-400 cm^{-1} region were measured to observe conformational changes in the peptides upon exposure to aqueous buffer.

Two buffers of different ionic compositions were used: 50 mM Na,K-phosphate (pD 7.2) + 50 mM NaCl, and 10 mM Na,K-phosphate (pD 7.2). Both buffers were prepared using D_2O, and pD was adjusted using a regular pH-meter, taking into account a 0.4 pH unit isotopic shift.[67] Reference spectra were measured using a single CaF_2 window for the dry samples and the respective blank buffer between two windows for samples in aqueous buffer. The instrument was purged with dry air throughout the measurements. Absorbance spectra of atmospheric water vapor were measured separately and used to correct the sample spectra when necessary. The final absorbance spectra of the peptide samples were smoothed using a 13-point Savitzky-Golay linear least squares algorithm embedded in the Igor Pro 5.03 software, and baseline corrected. In order to compare spectral line-shapes and calculate spectral differences, all spectra were normalized by dividing each spectrum by its amide I area, using Igor Pro 5.03.

Curve-fitting was performed using GRAMS spectroscopic software to estimate the fractions of various secondary structures in the peptides. The locations of the amide I components were determined based on the second derivatives. The result of the curve-fitting

procedure was considered satisfactory when the peak wavenumbers of the components agreed with those predicted by the second derivatives, the "curvefit," i.e. the sum of all components, reasonably fitted the actual spectrum , and the widths of the components were within meaningful limits.

3. Results and discussion

FTIR and CD have been used to assess the structural transitions in the unmodified and pyroglutamylated Aβ peptides during aggregation in aqueous buffers. The peptides were dissolved in HFIP to disperse pre-existing aggregates[66] and dried by desiccation. The secondary structure of the dehydrated peptides was determined, followed by addition of aqueous buffers of various ionic strengths and monitoring conformational transitions upon aggregation. Since Aβ is derived from APP, involving part of its transmembrane domain, the dehydrated peptide may mimic the peptide sequestered from the aqueous phase into the cell plasma membrane. The observed structural changes initiated by addition of the aqueous buffer mimic the conformational transitions of the peptides upon transfer to the cytosol or the extracellular milieu. It has been demonstrated that $A\beta_{1\text{-}42}$ or $A\beta pE_{3\text{-}42}$ form oligomers upon incubation in aqueous media at concentrations 10-100 μM and temperatures 25-37^{o}C for 2 hours or less, and the onset of fibrillogenesis occurs beyond the first two hours.[66,68-70] Hence, we have employed a biophysical approach to characterize the structural transitions from the α-helical monomeric structure to the initial oligomers of mostly β-sheet structure within this time frame.

3.1. Dehydrated peptides adopt α-helical conformation

3.1.1. Unlabeled peptides

To monitor the structural changes in the peptides during aggregation in an aqueous medium, their secondary structure was determined in HFIP, after solvent removal by desiccation, and during the first 2 hours of exposure to an aqueous buffer. The CD spectra of $A\beta_{1\text{-}42}$, $A\beta pE_{3\text{-}42}$, and their equimolar combination dissolved in HFIP all showed a minimum around 203 nm and a prominent shoulder around 220 nm (Figure 1a), indicative of irregular and α-helical conformations, respectively.[71-73] This is consistent with earlier CD and NMR data indicating predominantly α-helical structure for $A\beta_{1\text{-}42}$ in pure HFIP[66] or HFIP/H_2O media at high HFIP content[59] and for $A\beta pE_{3\text{-}40}$ in 40% trifluoroethanol/60% water.[62] Upon removal of the solvent, the dry peptides assume mostly α-helical structure with CD minima at 208-209 nm and 221-224 nm (Figure 1b-d). These data imply an intrinsic α-helical propensity of both peptides in a desolvated state. Addition of aqueous buffer to the dry peptides induces α-helix to β-sheet structural transition. The spectra of $A\beta_{1\text{-}42}$ acquire a well-defined β-sheet line-shape with a minimum at 215 nm upon exposure to water for 10 min, which undergoes little change during incubation for 2 hours (Figure 1b). The behavior of $A\beta pE_{3\text{-}42}$ is different; at 10 min of incubation in the aqueous buffer it retains significant α-helical structure, as evidenced by double minima around 206 and 221 nm, followed by gradual transition to β-sheet upon further exposure to water (Figure 1c). The equal molar combination of the two peptides displays a structural behavior similar to that of $A\beta pE_{3\text{-}42}$, i.e., a slower conversion to β-sheet and longer retention of the

intermediate α-helical structure (*cf*. gray spectra in Figure 1c and 1d). (CD spectra have been measured every 10 min; the intermediate spectra are omitted for clarity).

FTIR spectroscopy was used to further analyze the structural transitions in the peptides. The peptides dried from HFIP on an FTIR CaF_2 window demonstrate mostly α-helical structure with prominent peaks at 1658-1662 cm^{-1} (Figure 2). These peak wavenumbers are close to those measured for other α-helical peptides corresponding to phospholamban[74,75] or the transmembrane domain of influenza hemagglutinin.[76] Fractions of α-helix in the peptide samples were determined by curve-fitting and ranged from 57% to 86% (not shown). Other amide I components were assigned to turns or irregular structures.

3.1.2. Isotopically labeled peptides

In addition to the unlabeled peptides, four segmentally ^{13}C,^{15}N-labeled peptides were studied. Each of the $A\beta_{1\text{-}42}$ and $A\beta pE_{3\text{-}42}$ peptides was labeled either at $K^{16}L^{17}V^{18}$ or $V^{36}G^{37}G^{38}V^{39}$ stretches. Site-directed labeling of proteins or peptides with stable isotopes such as ^{13}C or both ^{13}C and ^{15}N generates a characteristic, downshifted FTIR amide I signal and thereby allows one to probe the local secondary structure.[67,77-80] Moreover, vibrational couplings between amino acid residues of similar or different isotopic contents result in distinct spectral features which provide additional structural details.[80-83] Spectra were analyzed using a resolution enhancement procedure, *i.e.*, 2nd derivatives, where the spectral components appear as downward peaks. Despite the inherent noise in the 2nd derivative spectra, they show well defined features like the major α-helical component at 1658-1662 cm^{-1} (Figure S1 in Electronic Supplementary Information). The spectra of the samples containing peptides ^{13}C, ^{15}N-labeled at $K^{16}L^{17}V^{18}$ consistently display an additional component located at 1624-1628 cm^{-1}. This ~32 cm^{-1} downshift is less than expected based on an isolated harmonic oscillator model but is consistent with FTIR data on α-helical synthetic peptides ^{13}C-labeled at 1 to 4 residues.[76,77,79] The higher-than-expect vibrational frequency of the labeled residues most likely results from through H-bonding and/or through space vibrational coupling with the unlabeled residues. (In an α-helix stabilized by i+4 → i H-bonding, three consecutively labeled residues would be H-bonded to unlabeled residues.) The peptides labeled at $V^{36}G^{37}G^{38}V^{39}$, on the other hand, show weaker spectral features that are shifted further down to 1596-1602 cm^{-1} (Figure S1). Diminished intensity and frequency of these signals suggest that the C-terminus of the peptides is disordered and the respective peptide units behave like isolated oscillators. Earlier data indicating significant weakening of the relative intensity of the amide I component generated by ^{13}C-labeled α-helical peptide residues upon thermal melting[78-81] provide support for this conjecture. The amide II region shows a major band around 1546 cm^{-1} and a weaker component at lower wavenumbers around 1516 cm^{-1} for the labeled peptides (Figures 2 and S1). This splitting evidently results from both ^{13}C- and ^{15}N-labeling, but these signals are not diagnostic in terms of secondary structural characterization.

Thus, the peptides in dehydrated state adopt mostly α-helical structure that involves the $K^{16}L^{17}V^{18}$ sequence. The small fraction of unordered structure involves the $V^{36}G^{37}G^{38}V^{39}$ segment close to the C-terminus, and possibly a stretch downstream to $K^{16}L^{17}V^{18}$. This is in partial agreement with NMR data on the APP fragments comprising the $A\beta_{1\text{-}42}$ sequence,[41,42] which identified a bend near residues $G^{37}G^{38}$, and agrees with MD data on the initial α-helical structure of Aβ,[56-58] implying that the dry peptide is a biologically meaningful starting material to monitor structural changes upon aggregation in an aqueous medium. The relatively high amide

I peak wavenumbers of the peptides (~1660 cm^{-1}) as compared with those of stable α-helices (1647-1657 cm^{-1})[67,84] suggest that the helices formed by the dry peptides are flexible. (Weaker helical H-bonding corresponds to stronger C=O covalent bonding and consequently to higher vibrational frequencies.) This is also in line with the flexible nature of the helix in APP sequence corresponding to Aβ.[41,42]

3.2. Conformational changes in aqueous buffer

3.2.1. Unlabeled peptides

Transfer into aqueous buffer results in substantial conformational changes in $Aβ_{1-42}$ and $AβpE_{3-42}$ peptides and their equimolar combinations. The prominent amide I α-helical feature around 1660 cm^{-1} is replaced with two major components located near 1630 cm^{-1} and 1673 cm^{-1} (Figure 3), which are readily assigned to β-sheet and type I β-turn structures.[67,84] The spectra also display residual α-helical features around 1660 cm^{-1}, indicating that during the first two hours of aggregation the peptides are mostly in β-sheet conformation still retaining fractions of α-helix. Distinction between parallel *versus* antiparallel or in-register *versus* out-of-register β-sheets cannot be made based solely on the β-sheet wavenumber. On the other hand, the weak, higher frequency (1680-1695 cm^{-1}) component resulting from amide I splitting in antiparallel β-sheets is not resolved well enough apparently because of its diminutive extinction coefficient.[84,85] The nature of the β-sheets will be addressed below, based on the data on isotopically labeled peptides. Meanwhile, analysis of spectra of the unlabeled peptides provides the following structural information. First, the β-sheet wavenumbers decrease by 2-5 cm^{-1} during 2-hour incubation in a D_2O-based buffer, owing to amide H/D exchange, but still remain in the 1633-1628 cm^{-1} range. This strongly suggests that, within this time frame, the peptides form intramolecular rather than intermolecular β-sheets because the latter structures generate lower frequency signals in the 1613-1625 cm^{-1} range (see Ref. 67 and references therein). Inspection of amide II region of the spectra showed that the amide H/D exchange was close to completion at 2 h incubation in D_2O-based buffers (Figure S2), implying no further spectral shifts would be expected upon prolonged exposure to D_2O. Second, the peptides adopt a tertiary structure that is not packed too tightly to prevent solvent access to most of the residues. Third, the prominent β-turn components and significant α-helical fractions imply that the peptides fold into a mixed α/β-type structure such as those predicted by MD simulations and CD data for helix-to-fiber intermediates of Aβ.[57,58,86] Fourth, systematic spectral differences between $Aβ_{1-42}$, $AβpE_{3-42}$ and their combination provide insight into individual structural propensities of the two peptides and mutual structural effects. Finally, data obtained on peptides in buffers of different ionic strengths allow assessment of the role of ionic interactions in the observed structural transitions (see below).

In a buffer of near-physiological ionic strength, distinct spectral differences are seen between $AβpE_{3-42}$ and $Aβ_{1-42}$ peptides (Figure 3 a,b,c). The $AβpE_{3-42}$ peptide absorbs stronger in the α-helical region and weaker in the β-sheet region compared to $Aβ_{1-42}$. The equimolar combination of the two peptides shows even stronger α-helix feature than any of the two peptides, but also has more β-turn and less β-sheet structure. The (Aβ - AβpE) difference spectra presented in Figure S3a show a negative peak in the α-helical region (~1660 cm^{-1}) and a positive one in the β-sheet region (~1620 cm^{-1}), clearly indicating a higher α-helical and lower β-sheet

structure in $A\beta pE_{3-42}$ as compared to $A\beta_{1-42}$. The difference between the spectrum of the 1:1 molar combination of $A\beta pE_{3-42}$ and $A\beta_{1-42}$ and the normalized spectral sum of the two peptides, [1:1 – ½(Aβ + AβpE)], displays well-defined positive components near 1672 cm^{-1} and 1653 cm^{-1} and a negative component around 1626 cm^{-1} (Figure S3b). If both peptides retained their individual structures in the 1:1 combination, then these difference spectra would represent flat lines. The observed spectral features indicate significant conformational changes in one or both peptides caused by intermolecular interactions in the combined sample, *i.e.* increase in the α-helical and turn structures at the expense of β-sheets. The fact that the 1:1 combination spectrum resembles that of AβpE more than Aβ suggests that the pyroglutamylated peptide possesses a stronger capability of propagating its structural features into the mixed peptide sample. Interestingly, the α-helical component in the combined sample is shifted from ~1660 cm^{-1} down to ~1653 cm^{-1}, as also seen in the raw spectra of Figure 3 a,b,c. Since spectral subtractions involved spectra exposed to D_2O for similar time periods, this shift most likely reflects structural differences, such as helix stabilization in the combined peptide sample, rather than amide deuteration effects. The results of curve-fitting reflect these structural differences in a quantitative manner (Figure S4). These data are tabulated in Table 1 and indicate the presence of 10-20% α-helical structure during the first two hours of aggregation. A higher fraction of α-helix in $A\beta pE_{3-42}$ agrees with a slower β-sheet conversion of this peptide. In sum, in a near-physiological ionic strength buffer the $A\beta pE_{3-42}$ peptide resists conversion of α-helix to β-sheet more than the unmodified $A\beta_{1-42}$ peptide. In the 1:1 combination, this α-helical propensity is augmented, corroborating the notion that $A\beta pE_{3-42}$ is able to retard amyloid fibrillogenesis by opposing α-helix to β-sheet structural transition.[65]

The structural behavior of the peptides in a low ionic strength buffer is different. Under these conditions, $A\beta pE_{3-42}$ displays higher β-sheet structure and reduced fractions of β-turn, α-helix and irregular components compared to $A\beta_{1-42}$ (Figure 3 d,e,f and Table 1). The (Aβ - AβpE) difference spectra highlight these structural features by a positive component in the 1675-1646 cm^{-1} region, corresponding to β-turn, α-helix, and irregular structures, and a negative component around 1620-1626 cm^{-1}, corresponding to β-sheet (Figure S3c). These data suggest that a low ionic strength buffer promotes β-sheet formation in the pyroglutamylated peptide faster than in the unmodified peptide, in contrast to the trend in a near-physiological buffer. This result is further supported by the fact that in low ionic strength buffer the β-sheet component of $A\beta pE_{3-42}$ is shifted to lower wavenumbers compared to $A\beta_{1-42}$ (Figure 3 d,e,f), while the opposite is true in the higher ionic strength buffer (Figure 3 a,b,c). Moreover, the spectra of the 1:1 molar combination are similar to those of $A\beta_{1-42}$ (Figure 3 d,e,f), indicating a dominant structural effect of $A\beta_{1-42}$ in a low salt buffer. The [1:1 – ½(Aβ + AβpE)] spectra show positive peaks around 1672 cm^{-1} and 1645 cm^{-1} and a negative well around 1624 cm^{-1} (Figure S3d), *i.e.*, the overall fractions of β-turn and unordered structure are increased and the fraction of β-sheet is reduced in the combined peptide sample, a structural feature of $A\beta_{1-42}$ under these conditions.

3.2.2. Isotopically labeled peptides

Analysis of proteins or peptides by isotope-edited FTIR spectroscopy provides site-specific structural information as well as such details as parallel *versus* antiparallel or in-register *versus* out-of-register β-sheets.[80] For example, in aligned β-strands, through H-bonding or through space $^{13}C{=}O\text{-}^{13}C{=}O$ vibrational coupling between peptide units in adjacent strands results in

lower frequency (~1591-1594 cm^{-1}) amide I mode whereas in the absence of in-register alignment ^{13}C-^{12}C couplings generate higher frequency (~1601-1604 cm^{-1}) components of enhanced intensity.[47,82,83]

The amide I FTIR spectra of the peptides ^{13}C, ^{15}N-labeled either at $K^{16}L^{17}V^{18}$ or $V^{36}G^{37}G^{38}V^{39}$ display a major peak around 1628-1637 cm^{-1} and a well-defined component around 1670-1673 cm^{-1} (Figures 4, 5) that are assigned to β-sheet and β-turn structures, respectively, as in the case of unlabeled peptides. Comparison of these spectra with those of the unlabeled peptides (Figure 3) identifies an additional component near 1598-1604 cm^{-1} that is evidently generated by the isotope-labeled residues. Spectral features in the 1650-1660 cm^{-1} region indicate significant fractions of α-helix. The results of curve-fitting, shown in Figure S5, identify β-sheet, β-turn, and α-helical components in $A\beta_{1\text{-}42}$ and $A\beta pE_{3\text{-}42}$ peptides and their combinations. In certain cases, an additional component at 1642-1647 cm^{-1} was present, which most likely is generated by irregular (unordered) structure. The secondary structural contents of the isotope-labeled peptide samples agree with those of the unlabeled peptides (Table 1) when the component generated by the isotope-labeled segment around 1600 cm^{-1} is assigned to β-sheet structure (see below).

In the buffer of near-physiological ionic strength, the β-sheet wavenumber of $A\beta_{1\text{-}42}$ is 4-5 cm^{-1} lower than that of $A\beta pE_{3\text{-}42}$ at similar times of exposure to the buffer, suggesting faster β-sheet formation in the unmodified peptide. With peptides labeled at $K^{16}L^{17}V^{18}$ (Figure 4 a,b,c), the pyroglutamylated peptide has more α-helical structure whereas the unmodified peptide features more β-turn structure. In case of peptides labeled at $V^{36}G^{37}G^{38}V^{39}$, again the β-sheet component of the unmodified peptide is shifted toward lower frequencies, and $A\beta pE_{3\text{-}42}$ has more β-turn structure than $A\beta_{1\text{-}42}$ (Figure 4 d,e,f). The consensus is that, under these conditions, $A\beta_{1\text{-}42}$ undergoes a more efficient transition to β-sheet structure whereas $A\beta pE_{3\text{-}42}$ tends to retain more α-helix or turn structures. The spectra of 1:1 combinations of the two peptides labeled at $K^{16}L^{17}V^{18}$ resemble those of $A\beta pE_{3\text{-}42}$, suggesting the pyroglutamylated peptide may have a stronger potency to dictate it structural features within the mixed sample, in agreement with data on unlabeled peptides (Figure 3 a,b,c).

In the low ionic strength buffer, the β-sheet peak of the unmodified peptide occurs at similar or higher wavenumbers compared to $A\beta pE_{3\text{-}42}$, *i.e.*, in this case $A\beta pE_{3\text{-}42}$ undergoes β-sheet transition more readily (Figure 5). Also, $A\beta_{1\text{-}42}$ contains higher fractions of β-turn than $A\beta pE_{3\text{-}42}$. These structural features are in agreement with those obtained on the unlabeled peptides (Figure 3 d,e,f) and indicate that low ionic conditions facilitate β-sheet formation in $A\beta pE_{3\text{-}42}$ more than in $A\beta_{1\text{-}42}$. Given the notoriously unstable, polymorph-prone nature of the prefibrillar structural intermediates of Aβ peptide,[87-89] identification of distinct structural propensities in multiple experiments on peptides from different sources certainly adds credibility to the observed structural trends. It should be noted here that despite clear differences between β-sheet propensities, the relative contents of β-turn and α-helical structures vary within certain ranges, indicating low energy barrier between these structures and possibly related to the inherent structural polymorphism of Aβ peptides.

3.3. Structural models

The important question is what structural information is obtained from the analysis of the signals generated by the isotope-labeled amino acid residues. The signal of the labeled residues is

located at 1602 ±1 cm^{-1} for $A\beta_{1-42}$, $A\beta pE_{3-42}$, and their 1:1 combination. Considering the main β-sheet wavenumbers of 1628-1637 cm^{-1} and using a harmonic oscillator model, where the vibrational frequency of a diatomic molecule with masses m_1 and m_2 is proportional to $(1/m_1 + 1/m_2)^{1/2}$, one can expect $^{13}C{=}O$ vibrational wavenumbers around 1592-1600 cm^{-1}. On the other hand, the diagnostic signal of $^{13}C{=}O$-$^{13}C{=}O$ couplings in β-sheets is in the range of 1591-1594 cm^{-1} and that of ^{13}C-^{12}C couplings is within 1601-1604 cm^{-1} (see above). All this information leads to the following structural constraints for the early oligomers. First, the β-sheet wavenumbers of both unlabeled and labeled segments strongly suggest formation of intramolecular β-sheets, because intermolecular β-sheets absorb at lower frequencies (see section 3.2.1). Second, both $K^{16}L^{17}V^{18}$ and $V^{36}G^{37}G^{38}V^{39}$ segments are in β-sheet conformation. Third, all, or at least most, isotopically labeled amino acid residues are involved in $^{13}C{=}O$-$^{12}C{=}O$ rather than $^{13}C{=}O$-$^{13}C{=}O$ vibrational couplings. Fourth, considering the moderate size of the peptides, the large fraction of β-sheet (up to 70%), and the presence of considerable fraction of α-helix, intramolecular parallel β-sheet formation is hardly possible hence can be ruled out with high confidence. The structure of the monomer of Aβ can be roughly presented as a core β-hairpin composed of two strands and a turn or loop that may be stabilized by a salt bridge between Asp^{23} and Lys^{28} (see Ref. 90), and a short α-helix (Figure 6). This model is consistent with the aforementioned four constraints. The N-terminus appears to be the most likely segment to harbor the transient α-helix, which has been identified in this work and in earlier studies.[54-58]

How do the monomers aggregate into early oligomers? The absence of intermolecular H-bonding and the absence of $^{13}C{=}O$-$^{13}C{=}O$ vibrational couplings help to explore this question. Figure 7 presents a number of possibilities for oligomer formation *via* interactions between the core β-hairpin structures. Parallel in-register stacking of the β-sheets with the aggregation axis perpendicular to the hairpin plane (Figure 7a), reminiscent to the structure of fibrils, would generate strong through-space $^{13}C{=}O$-$^{13}C{=}O$ couplings. Antiparallel stacking would also involve such couplings between the $K^{16}L^{17}V^{18}$ segments (Figure 7 b). Since $^{13}C{=}O$-$^{13}C{=}O$ coupling has not been seen, these two models are invalid. The next two models involve aggregation through non-H-bonding (i.e., ionic or hydrophobic) interactions between the N-terminal strand of one peptide and the C-terminal strand of the other, either in parallel or antiparallel arrangements (Figure 7 c,d). The two strands from neighboring hairpins that are involved in intermolecular interactions can be arranged either laterally, like in regular β-sheets, or stacked like in steric zippers,[91] possibly involving side chain interdigitation. Stacking can proceed alternately, when each hairpin has one strand above and the other below the neighboring strands (Figure 7 c), or the whole hairpins themselves can go up and down consecutively (Figure 7 d). Other geometries are possible, such as a staircase architecture where each hairpin goes up by one step. These structures are plausible because they involve $^{13}C{=}O$-$^{12}C{=}O$ and not $^{13}C{=}O$-$^{13}C{=}O$ couplings, in agreement with the data. Next we consider formation of dimers by interactions between the N-terminal strands or between C-terminal strands, followed by propagation of aggregation by interactions between C-terminal strands or N-terminal strands, parallel (Figure 7 e) or antiparallel (Figure 7 f). These structures predict $^{13}C{=}O$-$^{13}C{=}O$ couplings, which is not seen. Thus, peptide oligomers most likely form through interaction schemes shown in Figure 7 c,d.

The data suggest that in a buffer of near-physiological ionic strength $A\beta_{1-42}$ undergoes α-helix to β-sheet transition more readily than $A\beta pE_{3-42}$, while the opposite is true under low ionic strength conditions (Figures 3-5, Table 1). The presence of a residual α-helix in the transient structure of the peptide is likely to hinder β-sheet formation and aggregation (see Figure 6). The

protofibrils and fibrils do not contain any α-helix, *i.e.* this structure disappears along the way of fibrillogenesis. It is logical to assume that at low ionic strength the helix in $A\beta_{1\text{-}42}$ is more stable than in $A\beta pE_{3\text{-}4}$, while at higher ionic strength it becomes less stable. These effects are likely associated with the difference in charge of the N-termini of $A\beta_{1\text{-}42}$ and $A\beta pE_{3\text{-}42}$. According to the model presented in Figure 6, the N-terminal helix would be stabilized by a set of side chain ionic contacts, such as Asp^1-Lys^{16}, Glu^3-Lys^{16}, Asp^1-Arg^5, Arg^5-Glu^{11}. These ionic interactions would be strengthened under low ionic strength conditions, thus stabilizing the helical structure and retarding β-sheet formation. Helix-stabilizing ionic interactions involving Asp^1 and Glu^3 would not occur in $A\beta pE_{3\text{-}42}$ where Asp^1 is removed and Glu^3 is cyclized. These considerations provide a plausible explanation for a slower α-helix to β-sheet transition for $A\beta_{1\text{-}42}$ compared to $A\beta pE_{3\text{-}42}$ at low ionic strength and an opposite trend at higher ionic strength. This conclusion is in accord with earlier findings suggesting that the N-terminus of Aβ peptide controls the transition of the oligomers into protofibrils.[52] Further exploration of the mechanism of distinct structural propensities of the unmodified and pyroglutamylated Aβ peptides and the location of the transient α-helix will require additional research, involving peptides isotopically labeled within the N-terminus.

4. Conclusions

Aβ peptides originate from APP, including its α-helical transmembrane domain, and undergo complex, evidently multistep conformational changes leading to the formation of extracellular amyloid plaques, the hallmark of AD. These transitions include the initial α-helix to β-sheet conversion, dimerization, formation of early oligomers that are the most toxic species, further aggregation into protofibrils and final fibrillogenesis. While the mature fibrils have been very well structurally characterized, structural studies on the oligomers have proved more challenging mainly because of their unstable, dynamic nature, especially for time-consuming methods such as NMR. Here we have employed isotope-edited FTIR to capture the initial structural changes in $A\beta_{1\text{-}42}$ and the pyroglutamylated peptide $A\beta pE_{3\text{-}42}$, *i.e.* a transition from mostly α-helical structure to mostly β-sheet structure. Data on unlabeled peptides and those ^{13}C,^{15}N-labeled at two distinct segments have allowed identification of the most plausible modes of oligomer formation. Distinct differences have been detected between α-helix and β-sheet propensities of $A\beta_{1\text{-}42}$ and $A\beta pE_{3\text{-}42}$ and transitions from the former to the latter in two buffers of different ionic strengths. These data imply involvement of ionic interactions in α-helix to β-sheet transitions, and the observed ionic strength dependence of the structural transitions are likely associated with the loss of anionic charges of Asp^1 and Glu^3 side chains in $A\beta pE_{3\text{-}42}$. Structural models have been generated for the peptide monomers and oligomers (Figures 6, 7). Oligomers form by lateral or partially stacked non-H-bonding (*i.e.* ionic and/or nonpolar staggering) interactions between the N-terminal strand of one peptide monomer with the C-terminal strand of the other in parallel or antiparallel manner. These early oligomers, still retaining considerable fractions of α-helix, apparently contribute to Aβ cytotoxicity and their structural characterization is important to understand the mechanism of their toxic impact. While the present work identifies important structural constraints for the oligomers, further studies, involving isotopic labeling at additional segments, including the N-terminus, plus studies by higher resolution methods such as NMR, will lead to a better understanding of the structural basis of cytotoxicity of the unmodified and pyroglutamylated Aβ peptides.

5. Acknowledgements

This work was partially supported by NIH grant 1R03AI097591 and SEED grant from the College of Sciences of the University of Central Florida. Financial assistance from Dr. Bo Chen (Department of Physics, University of Central Florida) in purchasing the isotopically labeled peptides is gratefully acknowledged.

References

1. D. R. Thal, J. Walter, T. C. Saido and M. Fändrich, *Acta Neuropathol.,* 2015, **129,** 167-182.
2. J. Hardy and D. Allsop, *Trends Pharmacol. Sci.,* 1991, **12,** 383-388.
3. C. J. Pike, D. Burdick, A. J. Walencewicz, C. G. Glabe and C. W. Cotman, *J. Neurosci.,* 1993, **13,** 1676-87.
4. D. W. Dickson, *Neurobiol. Aging,* 1997, **18,** S21-S26.
5. M. D. Kirkitadze, G. Bitan and D. B. Teplow, *J. Neurosci. Res.,* 2002, **69,** 567-577.
6. W. L. Klein, W. B. Stine and D. B. Teplow, *Neurobiol. Aging.,* 2004, **25,** 569-580.
7. R. Resende, E. Ferreiro, C. Pereira and C. Resende de Oliveira, *Neuroscience,* 2008. **155,** 725-737.
8. S. L. Bernstein, N. F. Dupuis, N. D. Lazo, T. Wyttenbach, M. M. Condron, G. Bitan, D. B. Teplow, J. E. Shea, B. T. Ruotolo, C. V. Robinson and M. T. Bowers, *Nat. Chem.,* 2009, **1,** 326-331.
9. C. L. Masters and D. J. Selkoe, *Cold Spring Harb. Perspect. Med.*, 2012, 2:a006262, doi: 10.1101/cshperspect.a006262.
10. I. Benilova, E. Karran and B. De Strooper, *Nat. Neurosci.,* 2012, **15,** 349-357.
11. W. M. Tay, D. Huang, T. L. Rosenberry and A. K. Paravastu, *J. Mol Biol.,* 2013, **425,** 2494-2508.
12. A. Sebollela, G. M. Mustata, K. Luo, P. T. Velasco, K. L. Viola, E. N. Cline, G. S. Shekhawat, K. C. Wilcox, V. P. Dravid and W. L. Klein, *ACS Chem. Neurosci.,* 2014, **5,** 1238-1245.
13. E. Cerasoli, M. G. Ryadnov and B. M. Austen, *Front. Chem.,* 2015, **3,** 17. doi: 10.3389/fchem.2015.00017.
14. R. Lal, H. Lin and A. P. Quist, *Biochim. Biophys. Acta,* 2007, **1768,** 1966-1975.
15. N. Arispe, J. C. Diaz and O. Simakova, *Biochim. Biophys. Acta,* 2007, **1768,** 1952-1965.
16. A. L. Gillman, H. Jang, J. Lee, S. Ramachandran, B. L. Kagan, R. Nussinov and F. Teran Arce, *J. Phys. Chem. B,* 2014, **118,** 7335-7344.
17. E. Ferreiro, C. R. Oliveira and C. M. Pereira, *Neurobiol. Dis.*, 2008, **30,** 331-342.
18. E. Ferreiro, I Baldeiras , I. L. Ferreira, R. O. Costa, A. C. Rego, C. F. Pereira and C. R. Oliveira, *Int. J. Cell Biol.,* 2012, 735206. doi: 10.1155/2012/735206.
19. A. Demuro and I. Parker, *J. Neurosci.,* 2013, **33,** 3824-3833.
20. P. H. Reddy, R. Tripathi, Q. Troung, K. Tirumala, T. P. Reddy, V. Anekonda, U. P. Shirendeb, M. J. Calkins, A. P. Reddy, P. Mao and M. Manczak, *Biochim. Biophys. Acta,* 2012, **1822,** 639-649.
21. L. Pagani and A. Eckert, *Int. J. Alzheimers Dis,* 2011, 925050. doi: 10.4061/2011/925050.
22. S. C. Correia, R. X. Santos, M. S. Santos, G. Casadesus, J. C. Lamanna, G. Perry, M. A. Smith and P. I. Moreira, *Curr. Alzheimer Res.,* 2013, **10,** 406-419.

23. T. Y. Chi, L. H. Wang, X. F. Ji, L. Shen and L. B. Zou, *J. Asian Nat. Prod. Res.,* 2013, **15,** 1013-1022.
24. H. Lei, C. Y. Zhao, D. M. Liu, Y. Zhang, L. Li, X. L. Wang and Y. Peng, *J. Asian Nat. Prod. Res.,* 2014, **16,** 854-864.
25. R. Malinow, *Curr. Opin. Neurobiol.,* 2012, **22,** 559-563.
26. T. Kim, G. S. Vidal, M. Djurisic, C. M. William, E. Michael, M. E. Birnbaum, K. C. Garcia, B. T. Hyman, J. Carla and C. J. Shatz, *Science,* 2013, **341,** 1399-1404.
27. M. A. Fernandez, J. A. Klutkowski, T. Freret and M. S. Wolfe, *J. Biol. Chem,* 2014, **289,** 31043-31052.
28. T. A. Bayer and O. Wirths, *Acta Neuropathol.,* 2014, **127,** 787-801.
29. J. M. Nussbaum, S. Schilling, H. Cynis, A. Silva, E. Swanson, T. Wangsanut, K. Tayler, B. Wiltgen, A. Hatami, R. Rönicke, K. Reymann, B. Hutter-Paier, A. Alexandru, W. Jagla, S. Graubner, C. G. Glabe, H. U. Demuth and G. S. Bloom, *Nature,* 2012, **485,** 651-655.
30. T. C. Saido, T. Iwatsubo, D. M. Mann, H. Shimada, Y. Ihara and S. Kawashima, *Neuron,* 1995, **14,** 457-466.
31. G. Wu, R. A. Miller, B. Connolly, J. Marcus, J. Renger and M. J. Savage, *Neurodegener. Dis.,* 2014, **14,** 53-66.
32. Y. M. Kuo, M. R. Emmerling, A. S. Woods, R. J. Cotter and A. E. Roher, *Biochem. Biophys. Res. Commun.*, 1997, **237,** 188-191.
33. R. Perez-Garmendia and G. Gevorkian, *Curr. Neuropharmacol.,* 2013, **11,** 491-498.
34. C. Russo, E. Violani, S. Salis, V. Venezia, V. Dolcini, G. Damonte, U. Benatti, C. D'Arrigo, E. Patrone, P. Carlo and G. Schettini, *J. Neurochem.,* 2002, **82,** 1480-1489.
35. W. He and C. J. Barrow, *Biochemistry*, 1999, **38,** 10871-10877.
36. D. Schlenzig, S. Manhart, Y. Cinar, M. Kleinschmidt, G. Hause, D. Willbold, S. A. Funke, S. Schilling and H. U. Demuth, *Biochemistry*, 2009, **48,** 7072-7078.
37. D. Schlenzig, R. Rönicke, H. Cynis, H. H. Ludwig, E. Scheel, K. Reymann, T. Saido, G. Hause, S. Schilling and H. U. Demuth, *J. Neurochem.,* 2012, **121,**774-784.
38. C. D'Arrigo, M. Tabaton and A. Perico, *Biopolymers,* 2009, **91,** 861-873.
39. S. Jawhar, O. Wirths and T. A. Bayer, *J. Biol. Chem.,* 2011, **286,** 38825-38832.
40. M. Mandler, L. Walker, R. Santic, P. Hanson, A. R. Upadhaya, S. J. Colloby, C. M. Morris, D. R. Thal, A. J. Thomas, A. Schneeberger and J. Attems, *Acta Neuropathol.,* 2014, **128,** 67-79.
41. K. D. Nadezhdin, O. V. Bocharova, E. V. Bocharov, and A. S. Arseniev, *Acta Naturae,* 2011, **3,** 69-76.
42. P. J. Barrett, Y. Song, W. D. Van Horn, E. J. Hustedt, J. M. Schafer, A. Hadziselimovic, A. J. Beel and C. R. Sanders, *Science,* 2012, **336,** 1168-1171.
43. A. T. Petkova, Y. Ishii, J. J. Balbach, O. N. Antzutkin, R. D. Leapman, F. Delaglio and R. A. Tycko, *Proc. Natl. Acad. Sci. USA,* 2002, **99,** 16742-16747.
44. A. K. Paravastu, R. D. Leapman, W. M. Yau and R. Tycko, *Proc. Natl. Acad. Sci. USA,* 2008, **105,** 18349-18354.
45. T. Lührs, C. Ritter, M. Adrian, D. Riek-Loher, B. Bohrmann, H. Döbeli, D. Schubert and R. Riek, *Proc. Natl. Acad. Sci. USA,* 2005, **102,** 17342-17347.
46. Y. S. Kim, L. Liu, P. H. Axelsen and R. M. Hochstrasser, *Proc. Natl. Acad. Sci. USA,* 2008, **105,** 7720-7725.
47. C. Paul and P. H. Axelsen, *J. Am. Chem. Soc.,* 2005, **127,** 5754-5755.

48. J. J. Balbach, A. T. Petkova, N. A. Oyler, O. N. Antzutkin, D. J. Gordon, S. C. Meredith and R. Tycko, *Biophys. J*. 2002, **83,** 1205-1216.
49. M. Ahmed, J. Davis, D. Aucoin, T. Sato, S. Ahuja, S. Aimoto, J. I. Elliott, W. E. Van Nostrand and S. O. Smith, *Nat. Struct. Mol. Biol.,* 2010, **17,** 561-567.
50. S. Chimon, M. A. Shaibat, C. R. Jones, D. C. Calero, B. Aizezi and Y. Ishii, *Nat. Struct. Mol. Biol.,* 2007, **14,** 1157-1164.
51. L. Yu, R. Edalji, J. E. Harlan, T. F. Holzman, A. P. Lopez, B. Labkovsky, H. Hillen, S. Barghorn, U. Ebert, P. L. Richardson, L. Miesbauer, L. Solomon, D. Bartley, K. Walter, R. W. Johnson, P. J. Hajduk and E. T. Olejniczak, *Biochemistry,* 2009, **48,** 1870-1877.
52. C. Haupt, J. Leppert, R. Rönicke, J. Meinhardt, J. K. Yadav, R. Ramachandran, O. Ohlenschläger, K. G. Reymann, M. Görlach and M. Fändrich, *Angew. Chem. Int. Ed. Engl.,* 2012, **51,** 1576-1579.
53. H. A. Scheidt, I. Morgado, S. Rothemund, D. Huster and M. Fändrich, *Angew. Chem. Int. Ed. Engl.,* 2011, **50,** 2837-2840.
54. M. D. Kirkitadze, M. M. Condron and D. B. Teplow, *J. Mol. Biol.,* 2001, **312,** 1103-1119.
55. K. Ono, M. M. Condron and D. B. Teplow, *Proc. Natl. Acad. Sci. USA,* 2009, **106,** 14745-14750.
56. B. Urbanc, L. Cruz, F. Ding, D. Sammond, S. Khare, S. V. Buldyrev, H. E. Stanley and N. V. Dokholyan, *Biophys. J.,* 2004, **87,** 2310-2321.
57. Y. Xu, J. Shen, X. Luo, W. Zhu, K. Chen, J. Ma and H. Jiang, *Proc. Natl. Acad. Sci. USA.,* 2005, **102,** 5403-5407.
58. A. Vandersteen, M. F. Masman, G. De Baets, W. Jonckheere, K. van der Werf, S. J. Marrink, J. Rozenski, I. Benilova, B. De Strooper, V. Subramaniam, J. Schymkowitz, F. Rousseau and K. Broersen, *J. Biol. Chem.,* 2012, **287,** 36732-36743.
59. S. Tomaselli, V. Esposito, P. Vangone, N. A. van Nuland, A. M. Bonvin, R. Guerrini, T. Tancredi, P. A. Temussi and D. Picone, *ChemBioChem,* 2006, **7,** 257-267.
60. A. Abedini and D. P. Raleigh, *Protein Eng. Des. Sel.,* 2009, **22,** 453-459.
61. E. Cerf, R. Sarroukh, S. Tamamizu-Kato, L. Breydo, S. Derclaye, Y. F. Dufrêne, V. Narayanaswami, E. Goormaghtigh, J. M. Ruysschaert and V. Raussens, *Biochem. J.,* 2009, **421,** 415-423.
62. N. Sun, R. Hartmann, J. Lecher, M. Stoldt, S. A. Funke, L. Gremer, H. H. Ludwig, H. U. Demuth, M. Kleinschmidt and D. Willbold, *J. Pept. Sci.,* 2012, **18,** 691-695.
63. T. L. Tekirian, A. Y. Yang, C. Glabe and J. W. Geddes, *J. Neurochem.,* 1999, **73,** 1584-1589.
64. H. M. Sanders, R. Lust and J. K. Teller, *Peptides,* 2009, **30,** 849-854.
65. J. O. Matos, G. Goldblatt, J. Jeon, B. Chen and S. A. Tatulian, *J. Phys. Chem. B,* 2014, **118,** 5637-5643.
66. W. B. Stine Jr., K. N. Dahlgren, G. A. Krafft and M. J. LaDu, *J. Biol. Chem.,* 2003, **278,** 11612-11622.
67. S. A. Tatulian, *Methods Mol. Biol.,* 2013, **974,** 177-218.
68. S. Schilling, T. Lauber, M. Schaupp, S. Manhart, E. Scheel, G. Böhm and H. U. Demuth, *Biochemistry,* 2006, **45,** 12393-12399.
69. Y. Bouter, K. Dietrich, J. L. Wittnam, N. Rezaei-Ghaleh, T. Pillot, S. Papot-Couturier, T. Lefebvre, F. Sprenger, O. Wirths, M. Zweckstetter and T. A. Bayer, *Acta Neuropathol.,* 2013, **126,** 189-205.
70. N. Salvadores, M. Shahnawaz, E. Scarpini, F. Tagliavini and C. Soto, *Cell Rep.,* 2014, **7,** 261-268.

71. N. Sreerama and R. W. Woody, in *Circular Dichroism: Principles and Applications,* ed. N. Berova, K. Nakanishi and R. W. Woody, John Wiley & Sons, Hoboken, N.J., 2000, pp. 601-620.
72. S. M. Kelly and N. C. Price, *Curr. Protein Pept. Sci.,* 2000, **1,** 349-384.
73. K. Bakshi, M. R. Liyanage, D. B. Volkin and C. R. Middaugh, *Methods Mol. Biol.,* 2014, **1088,** 247-253.
74. C. F. Ludlam, I. T. Arkin, X. M. Liu, M. S. Rothman, P. Rath, S. Aimoto, S. O. Smith, D. M. Engelman and K. J. Rothschild, *Biophys. J.,* 1996, **70,** 1728-1736.
75. S. A. Tatulian, L. R. Jones, L. G. Reddy, D. L. Stokes and L. K. Tamm, *Biochemistry,* 1995, **34,** 4448-4456.
76. S. A. Tatulian and L. K. Tamm, *Biochemistry,* 2000, **39,** 496-507.
77. S. Y. Venyaminov, J. F. Hedstrom and F. G. Prendergast, *Proteins,* 2001, **45,** 81–89.
78. R. Huang, J. Kubelka, W. Barber-Armstrong, R. A. G. D. Silva, S. M. Decatur and T. A. Keiderling, *J. Am. Chem. Soc.,* 2004, **126,** 2346-2354.
79. W. Barber-Armstrong, T. Donaldson, H. Wijesooriya, R. A. G. D. Silva and S. M. Decatur, *J. Am. Chem. Soc.,* 2004, **126,** 2339-2345.
80. S. M. Decatur, *Acc. Chem. Res.,* 2006, **39,** 169-175.
81. S. M. Decatur, *Biopolymers,* 2000, **54,** 180–185.
82. S. A. Petty and S. M. Decatur, *J. Am. Chem. Soc.,* 2005, **127,** 13488-13489.
83. S. A. Petty and S. M. Decatur, *Proc. Natl. Acad. Sci. USA.,* 2005, **102,** 14272-14277.
84. S. Krimm and J. Bandekar, *Adv. Protein Chem.,* 1986, **38,** 181-364.
85. S. Y. Venyaminov and N. N. Kalnin, *Biopolymers,* 1990, **30,** 1259-1271.
86. D. Liu, Y. Xu, Y. Feng, H. Liu, X. Shen, K. Chen, J. Ma, and H. Jiang, *Biochemistry,* 2006, **45,** 10963-10972.
87. A. T. Petkova, R. D. Leapman, Z. Guo, W. M. Yau, M. P. Mattson and R. Tycko, *Science,* 2005, **307,** 262-265.
88. J. S. Jeong, A. Ansaloni, R. Mezzenga, H. A. Lashuel and G. Dietler, *J. Mol. Biol.,* 2013, **425,** 1765-1781.
89. R. Tycko, *Neuron,* 2015, **86,** 632-645.
90. R. Tycko, *Annu. Rev. Phys. Chem.,* 2011 **62,** 279-299.
91. R. Nelson, M. R. Sawaya, M. Balbirnie, A. Ø. Madsen, C. Riekel, R. Grothe and D. Eisenberg, *Nature*, 2005, **435,** 773-778.

Figure Legends

Figure 1. (a) CD spectra of 50 μM peptide solutions in HFIP. Black solid, dotted, and gray solid lines correspond to $A\beta_{1\text{-}42}$, $A\beta pE_{3\text{-}42}$, and their 1:1 combination, respectively. Panels b), c), and d) present spectra of $A\beta_{1\text{-}42}$, $A\beta pE_{3\text{-}42}$, and their 1:1 combination, respectively, in dry state (black solid lines), 10 min in aqueous buffer (50 mM NaCl, 50 mM Na,K-phosphate, pH 7.2) (gray solid lines), and 2 h in buffer (dotted lines).

Figure 2. FTIR spectra of dry peptides in amide I and amide II regions. Spectra for unlabeled and isotopically labeled $A\beta_{1\text{-}42}$ and $A\beta pE_{3\text{-}42}$ peptides and their 1:1 combinations are presented. Dotted lines correspond to $A\beta pE_{3\text{-}42}$, and solid lines correspond either to $A\beta_{1\text{-}42}$ or to combined samples, as indicated. KLV or VGGV imply the peptides have been labeled at $K^{16}L^{17}V^{18}$ or $V^{36}G^{37}G^{38}V^{39}$, respectively. In KLV/VGGV or VGGV/KLV samples, the first stretch applies to $A\beta_{1\text{-}42}$ and the second to $A\beta pE_{3\text{-}42}$. All spectra are normalized to a total area of 1.0.

Figure 3. FTIR spectra of unlabeled $A\beta_{1\text{-}42}$ (black solid line), $A\beta pE_{3\text{-}42}$ (dotted line), and their 1:1 combination (gray solid line) in D_2O-based buffers of 50 mM NaCl, 50 mM Na,K-phosphate, pD 7.2 (a,b,c) and 10 mM Na,K-phosphate (pD 7.2) (d,e,f) for 10 min (a,d), 1 h (b,e), and 2 h (c,f). All spectra are normalized to a total area of 1.0.

Figure 4. FTIR spectra of $A\beta_{1\text{-}42}$ (black solid line), $A\beta pE_{3\text{-}42}$ (dotted line), and their 1:1 combination (gray solid line) labeled either at $K^{16}L^{17}V^{18}$ (a, b, c) or $V^{36}G^{37}G^{38}V^{39}$ (d, e, f) in D_2O-based buffers of 50 mM NaCl, 50 mM Na,K-phosphate, pD 7.2, for 10 min (a,d), 1 h (b,e), and 2 h (c,f). Inset text in each panel intends to facilitate identification of spectra. For example, "AβpEVGGV 1 h" means $A\beta pE_{3\text{-}42}$ peptide labeled at $V^{36}G^{37}G^{38}V^{39}$ incubated in buffer for 1 h. All spectra are normalized to a total area of 1.0.

Figure 5. FTIR spectra of $A\beta_{1\text{-}42}$ (black solid line), $A\beta pE_{3\text{-}42}$ (dotted line), and their 1:1 combination (gray solid line) labeled either at $K^{16}L^{17}V^{18}$ (a, b, c) or $V^{36}G^{37}G^{38}V^{39}$ (d, e, f) in D_2O-based buffers of 10 mM Na,K-phosphate, pD 7.2, for 10 min (a,d), 1 h (b,e), and 2 h (c,f). Inset text is explained under Figure 4. All spectra are normalized to a total area of 1.0.

Figure 6. (a) The amino acid sequence of $A\beta_{1\text{-}42}$ arranged in a structure involving a β-hairpin stabilized by Asp^{23}-Lys^{28} ionic bridge, and an N-terminal stretch that may assume α-helical conformation. The isotopically labeled amino acids are shaded. (b) Ribbon model for Aβ monomer, composed of a β-hairpin and an N-terminal α-helix. The segments $K^{16}L^{17}V^{18}$ and $V^{36}G^{37}G^{38}V^{39}$ are both involved in the β-hairpin and are marked by dark blue color.

Figure 7. Schematic models for Aβ oligomerization through interactions between the core β-hairpin structures. Two arrows in each molecule represent two β-strands, connected by a loop or turn. The monomers are colored gray and pink, and the isotopically labeled segments are indicated by darker color. In all cases, the structures are stabilized by intramolecular H-bonding and intermolecular non-H-bonding contacts, *i.e.* ionic and/or hydrophobic interactions. The plane of the picture is parallel to the hairpin plane. In a) and b), the aggregation axis is perpendicular, and in c) to f) it is coplanar to the picture plane.

Table 1. Secondary structures of $A\beta_{1-42}$, $A\beta pE_{3-42}$, and their 1:1 combinations incubated in 50 mM NaCl + 50 mM Na,K-phosphate buffer (shaded rows) or 10 mM Na,K-phosphate buffer, pD 7.2, as determined by curve-fitting of FTIR amide I bands (see Figure S3). Average percentages for 10 min, 1 h, and 2 h incubation in aqueous media are presented. "Other" refers mostly to irregular structure.

	$A\beta_{1-42}$	$A\beta pE_{3-42}$	$A\beta_{1-42}$ /$A\beta pE_{3-42}$ (1:1)
α-helix	11.0±2.4	18.7±3.2	22.9±3.6
	24.8±5.1	13.6±1.8	16.3±2.1
β-sheet	50.4±4.6	43.0±4.4	34.5±3.9
	38.7±4.8	48.9±3.6	34.2±3.2
β-turn	18.1±3.3	20.3±1.7	28.4±2.4
	24.0±2.7	19.8±1.3	27.7±3.6
other	20.5±3.9	18.0±2.2	14.2±1.3
	12.5±3.6	17.7±2.6	21.8±2.7

Fig. 1

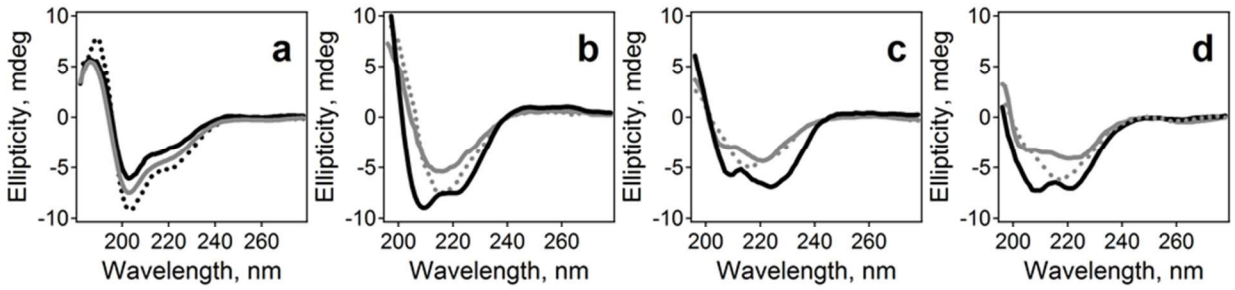

Fig. 2

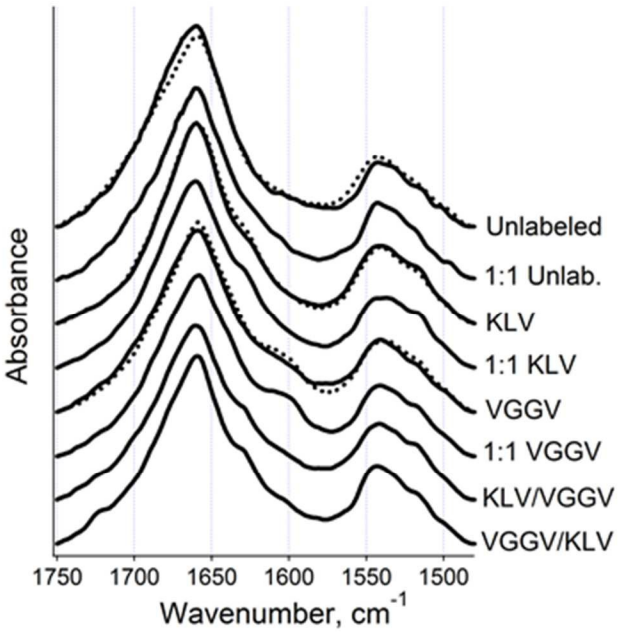

Fig. 3

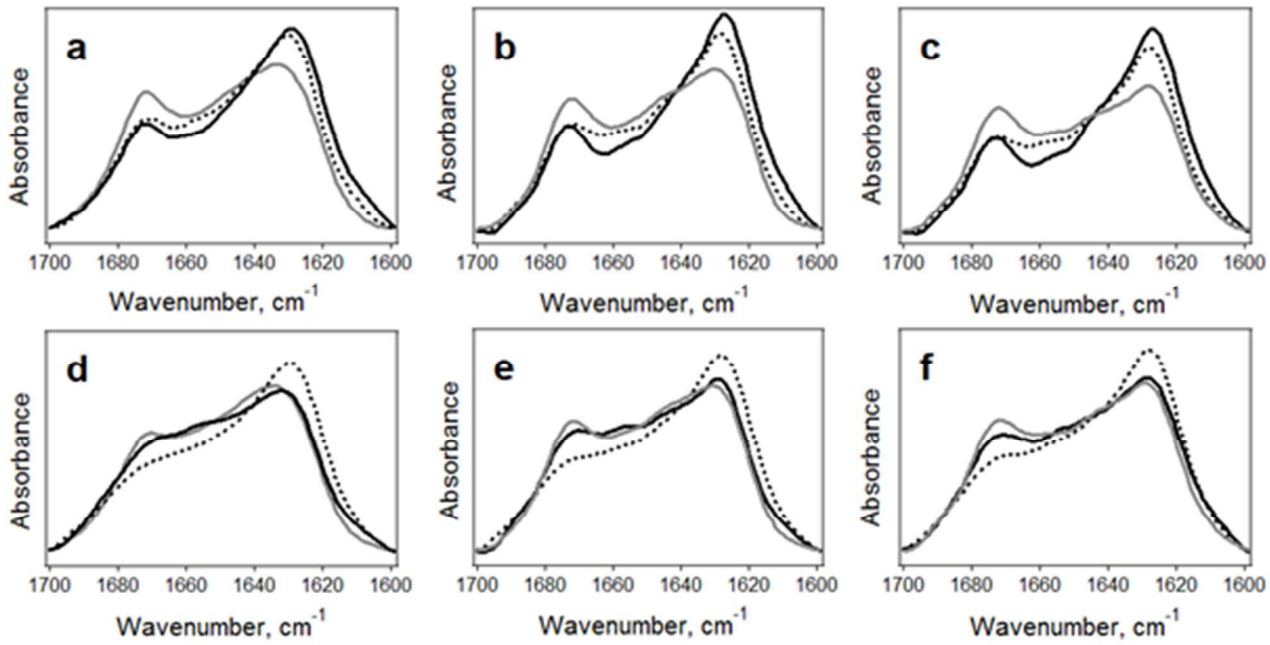

Fig. 4

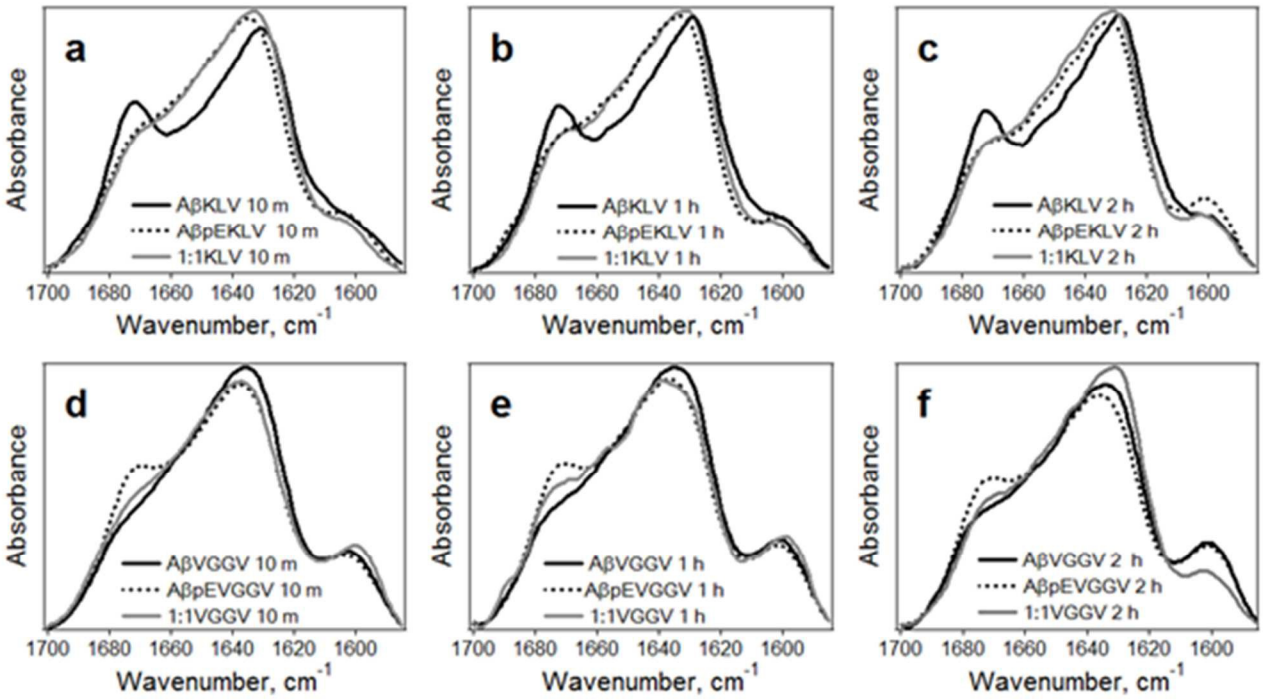

Fig. 5

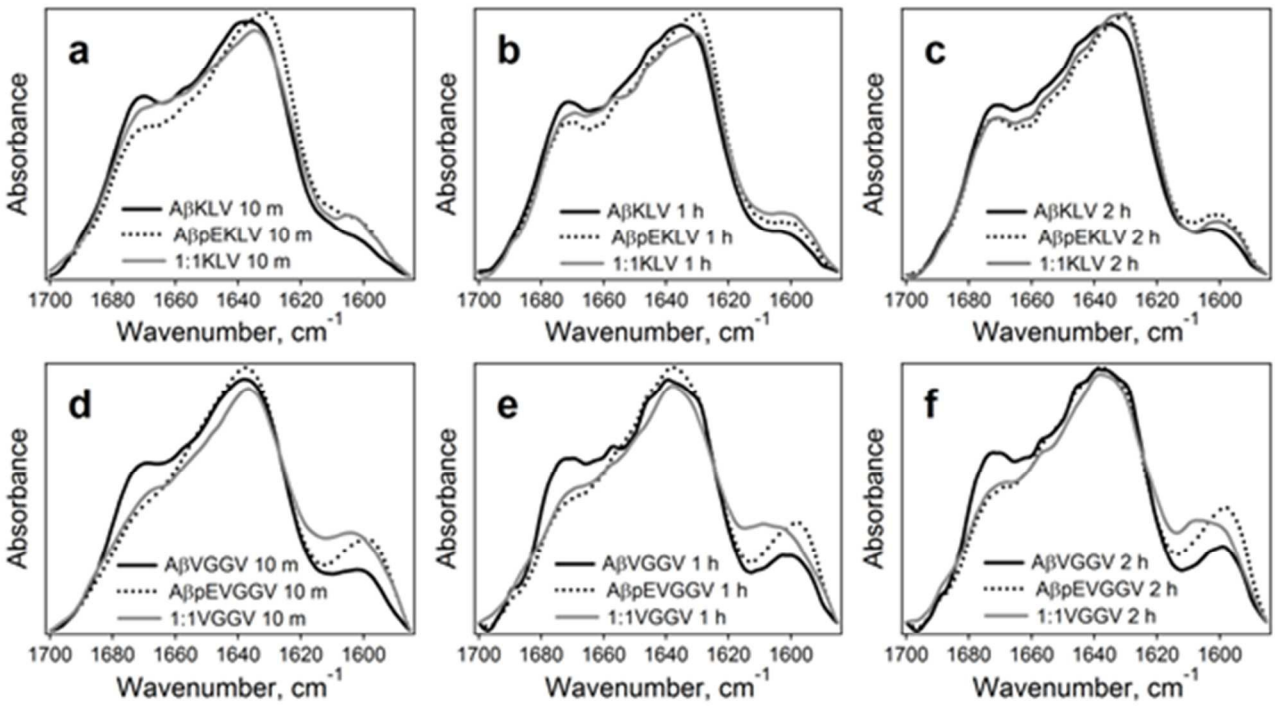

Fig. 6

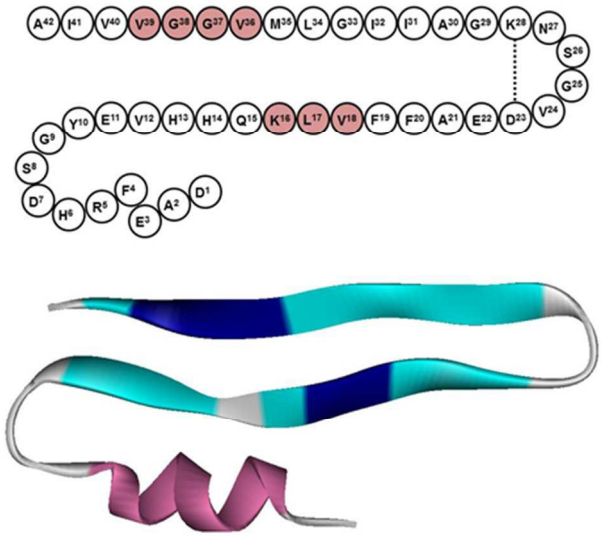

Fig. 7